

Radiative transitions in stacked type-II ZnMgTe quantum dots embedded in ZnSe

U. Manna, Q. Zhang, S. Dhomkar, I. F. Salakhutdinov, M. C. Tamargo et al.

Citation: *J. Appl. Phys.* **112**, 063521 (2012); doi: 10.1063/1.4754451

View online: <http://dx.doi.org/10.1063/1.4754451>

View Table of Contents: <http://jap.aip.org/resource/1/JAPIAU/v112/i6>

Published by the [American Institute of Physics](#).

Related Articles

Fabrication and photoluminescence of SiC quantum dots stemming from 3C, 6H, and 4H polytypes of bulk SiC
Appl. Phys. Lett. **101**, 131906 (2012)

Anomalous temperature dependence of photoluminescence in self-assembled InGaN quantum dots
Appl. Phys. Lett. **101**, 131101 (2012)

Optical properties of multi-stacked InGaAs/GaNAs quantum dot solar cell fabricated on GaAs (311)B substrate
J. Appl. Phys. **112**, 064314 (2012)

Tunable electroluminescence from polymer-passivated 3C-SiC quantum dot thin films
Appl. Phys. Lett. **101**, 123110 (2012)

Control of growth and the processes of energy transfer from CdSe quantum dots for Nd³⁺ ions in a vitreous system: Thermal annealing time
Appl. Phys. Lett. **101**, 121903 (2012)

Additional information on J. Appl. Phys.

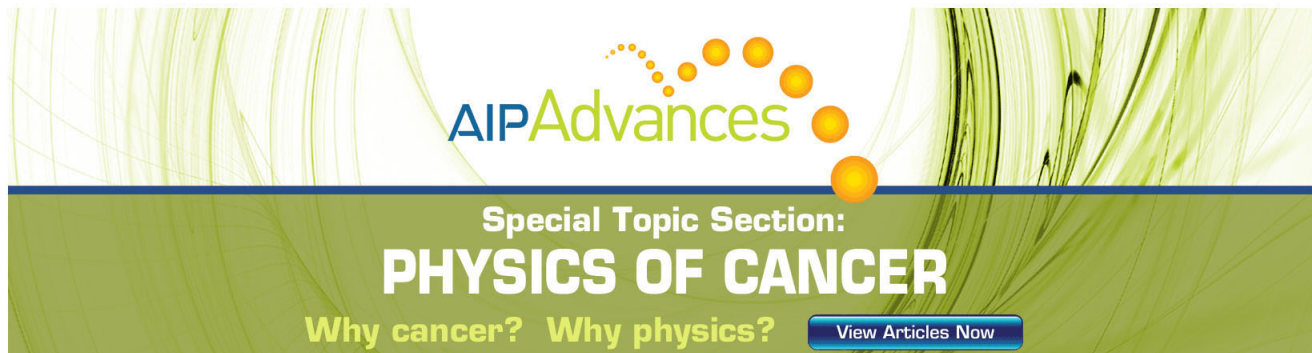
Journal Homepage: <http://jap.aip.org/>

Journal Information: http://jap.aip.org/about/about_the_journal

Top downloads: http://jap.aip.org/features/most_downloaded

Information for Authors: <http://jap.aip.org/authors>

ADVERTISEMENT



AIP Advances

Special Topic Section:
PHYSICS OF CANCER

Why cancer? Why physics? [View Articles Now](#)

Radiative transitions in stacked type-II ZnMgTe quantum dots embedded in ZnSe

U. Manna,^{1,a)} Q. Zhang,^{2,3} S. Dhomkar,^{3,4} I. F. Salakhutdinov,^{1,4} M. C. Tamargo,^{2,3}
I. C. Noyan,¹ G. F. Neumark,¹ and I. L. Kuskovsky^{3,4,b)}

¹*Department of Applied Physics and Applied Mathematics, Columbia University, New York, New York 10027, USA*

²*Department of Chemistry, City College of CUNY, New York, New York 10031, USA*

³*The Graduate Center, CUNY, 365 5th Avenue, New York, New York 10016, USA*

⁴*Department of Physics, Queens College of CUNY, Flushing, New York 11367, USA*

(Received 12 March 2012; accepted 24 August 2012; published online 25 September 2012)

Sub-monolayer quantities of Mg are introduced in multilayer stacked ZnMgTe quantum dots (QDs) embedded in ZnSe barriers in order to reduce the hole confinement energy by controlling the bandgaps and band-offsets of ZnTe/ZnSe system having type-II band alignment. The photoluminescence (PL) emission from such ZnMgTe/ZnSe QD structure is found to be a broad band centered at 2.35 eV. The higher energy side of the PL band shows a larger blue-shift with increasing excitation intensity and a faster life-time decay due to a greater contribution of the emission from the smaller size dots and the isoelectronic bound excitons. It is found that the characteristic decay time of the PL evolves along the band with a value of 129 ns at 2.18 eV to 19 ns at 2.53 eV. The temperature dependent PL emission is controlled by two thermally activated processes: ionization of electrons away from QD state to the barrier ($E_{A1} \sim 3$ meV) by breaking the type-II excitons and thermal escape of the holes from the ground state to the barrier ($E_{A2} \sim 114$ -116 meV). We propose a modified band diagram and energy levels for this ZnMgTe/ZnSe multilayer QD system by determining the composition of Mg inside the QDs and solving the 1-D Schrodinger's equation and show that Mg incorporation lowers the hole activation energy via modification of the valence band offset without changing the barrier significantly. © 2012 American Institute of Physics. [<http://dx.doi.org/10.1063/1.4754451>]

I. INTRODUCTION

The staggered band alignment of type-II semiconductor heterostructures leads to the spatial separation of photogenerated electrons and holes giving rise to an internal electric field that modifies the energy levels and wave functions of electron-hole pairs.^{1,2} The spatial separation of electrons and holes, thus enables one to tune the optical properties of type-II heterostructures and suppresses the non-radiative Auger recombination,³ which may lead to possible realization of advanced photonic and electronic devices, including improved solar cells based on intermediate band approach. Previously, ZnTe/ZnSe multiple quantum dot (QD), quantum well (QW), and superlattice (SL) structures with type-II band alignment have been grown in hopes of achieving tunable optical properties via quantum confinement effects.⁴⁻⁷

Apart from their optical tunability, ZnTe/ZnSe heterostructures are of interest for advancing the bipolar doping of “difficult to dope” ZnSe-based alloys,^{8,9} since the latter can be readily doped n-type, while ZnTe can be doped p-type. Introduction of sub-monolayer quantities of ZnTe within the ZnSe matrix led to the simultaneous formation of Te isoelectronic center and ZnTe rich QDs embedded in the ZnSe.^{5,8} Furthermore, doping of these QDs with nitrogen resulted in a higher p-type carrier concentration than those achieved in

ZnSe.^{8,9} However, due to a large hole confinement energy, the free carriers could not be readily observed. To further explore the possibility of enhancing p-type doping in this material system, as well as to investigate the limits of band gap engineering at the nanoscale, we have attempted to modify the QD band gap by incorporating sub-monolayer quantities of Mg along with Te using migration enhanced epitaxy (MEE), to form ZnMgTe QDs, instead of ZnTe QDs. The carrier confinement in type-II systems, such as Zn-Se-Te, is independent of the bandgaps of the underlying materials but rather depends on the band offsets. The choice of Mg is due to the absence of cation core *d*-electrons in MgTe, which while increases the bandgap, more importantly, lowers the valence band maximum relative to that of ZnTe,^{10,11} reducing the valence band offset (VBO) with ZnSe.^{11,12} Thus, incorporation of Mg in ZnTe is expected to reduce the hole confinement energy and enhance p-type conductivity. A hole free carrier concentration in the order of mid- 10^{15} cm⁻³ has been measured for the first time,¹³ in such samples.

Thus, incorporating Mg in this material system will allow us to control band offsets, and hence the confinement energies, as well as to engineer the ZnMgTe/ZnSe bandgaps. We propose that modification of the valence band-offsets in this material system will also allow us to create and control an intermediate band lying within the forbidden energy gap of these materials to absorb photon energies below the semiconductor bandgap and possibly increase the efficiency of intermediate band solar cells.¹⁴

^{a)}Electronic address: um2124@columbia.edu.

^{b)}Electronic address: Igor.Kuskovsky@qc.cuny.edu.

In this paper, we report detailed results of the “continuous wave” (cw) and “time-resolved” (TR-) photoluminescence (PL) spectroscopy of ZnMgTe/ZnSe multilayer QD structures with type-II band alignment grown by MEE under varying excitation and temperature with supporting results from the high resolution x-ray diffraction (HRXRD) studies. From the distribution of the coherent and diffuse x-ray scattering intensity in reciprocal space map (RSM), we show that the ZnMgTe QDs are vertically correlated along the growth direction; hence, an array of stacked QDs is formed within the structure. The size and composition fluctuation of stacked ZnMgTe QDs along with strong electron-phonon interactions cause a distribution of the density of states over a wide energy range resulting in a spectrally broad PL emission centered at 2.35 eV.

The excitation dependent PL shows distinctly different behavior at the lower energy side (LES) and higher energy side (HES) of the band. The low-energy side of the band, where the emission is dominated by larger dots follows a cube root dependence of excitation intensity and shows a smaller blue-shift (~ 12 meV) with increasing excitation intensity, varied over five orders of magnitude. The higher energy side of the band, where the emission is dominated by emission from smaller dots along with that from Te_n isoelectronic bound excitons (IBEs) located in ZnSe barrier, does not show a cube root dependence on the excitation intensity, while shows a larger blue-shift (~ 25 meV) under equal increase in the excitation intensity. At high excitation intensities, the decay time in ZnMgTe/ZnSe multilayer structure evolves from a non-exponential decay with a fast initial decay to an exponential decay with a much slower decay time at longer observation times. The characteristic decay time, $\tau_c \sim 129$ ns for a detection energy at the lower energy side of the band, is found to decrease monotonically with increasing detection energy across the PL spectrum.

Analysis of the temperature dependent PL intensity and decay time reveals that two thermally activated processes, ionization of electrons from QDs to the barrier by breaking the type-II excitons with an activation energy, $E_{A1} \sim 3$ meV, and ionization of holes, which thermally escape after making a transition from the QD ground state to the barrier with an activation energy, $E_{A2} \sim 114$ – 116 meV, are responsible for PL intensity quenching and decrease in decay time with increasing temperature. At maximum excitation intensity,

where contribution from the IBEs is relatively high, it is found that the IBE emission influences the temperature dependent behavior of the PL peak energy, the full-width at half maximum (FWHM), as well as the integrated intensity.

Finally, we determine the modified bandgaps and band-offsets of this ZnMgTe/ZnSe multilayer QD structure by determining the composition of the constituent elements from HRXRD measurement and estimate the QD energy levels by solving the 1-D Schrodinger’s equation for a square well potential. The results show that incorporation of Mg lowers the hole activation energy via modifying the confinement levels without changing the barrier properties in any significant manner.

II. EXPERIMENTAL

The multilayer ZnMgTe/ZnSe structure as schematically shown in Fig. 1(a) was grown on (001) GaAs substrates in a Riber 2300 molecular beam epitaxy (MBE) system by exposing the growing surface to alternate elements, commonly known as MEE following procedures described elsewhere.^{9,13,15} The GaAs substrate was exposed to a Zn-flux before the growth of a 5 nm ZnSe buffer layer at substrate temperature of 200 °C. After that, an undoped ZnSe buffer layer was grown at substrate temperature of 300 °C under Se rich conditions with a growth rate of ~ 0.3 $\mu\text{m/h}$. A streaky (2×1) RHEED pattern was observed after the buffer layer growth. After the growth of the barrier ZnSe (~ 10 MLs) by opening the Zn and Se shutters together for 35 s, ZnMgTe QDs were grown by employing three cycles of shutter operations as shown in Fig. 1(b). In cycle-1, following the ZnSe barrier growth, the Zn shutter was opened for 5 s followed by a 5 s growth interruption to desorb the excess Zn from the surface. After that, the Te shutter was opened to deposit Te on the Zn-terminated surface for 5 s, followed by another 5 s growth interruption. Cycle-2 was almost identical to cycle-1, except that during the deposition of Zn, the Mg shutter was opened simultaneously. Cycle-3 was identical to cycle-1. This shutter operation produces sequential deposition of the elements, which, combined with the short interruptions, gives rise to enhanced surface migration and the formation of self-assembled ZnMgTe QDs without formation of wetting layer, analogous to ZnTe QDs embedded in ZnSe.^{4,5,16}

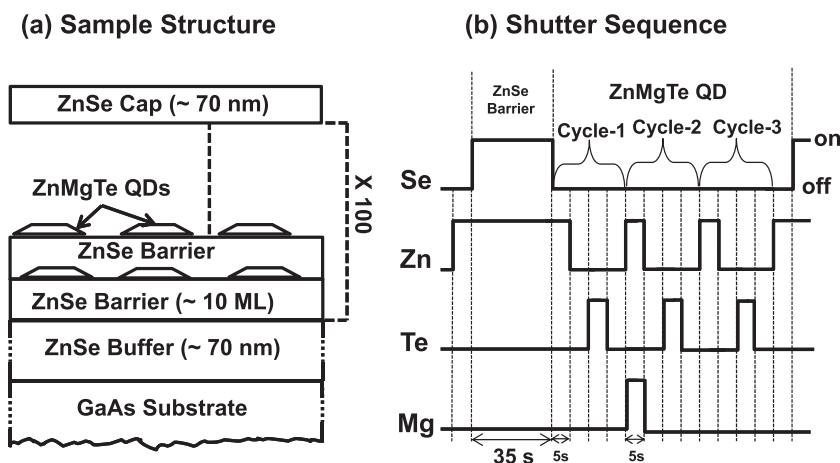


FIG. 1. (a) The sample structure and (b) shutter sequence employed during migration enhanced epitaxy growth of the ZnMgTe/ZnSe multilayers.

The advantage of such growth is that we can incorporate dopants, p-type, such as N in this case, directly into the QDs, and grow hundreds of layers containing QDs, potentially giving us a large number of energy states without wetting layers. The sequence of the ZnSe barrier and ZnMgTe QD depositions was repeated one hundred times for the sample studied here in order to obtain multi-layers thick enough for measurements. The transmission electron microscopy (TEM) images of the ZnMgTe/ZnSe sample¹⁷ clearly showed the presence of a modulated structure but did not reveal the presence of quantum dots directly because of the small size of the dots and low contrast between ZnSe and ZnMgTe. However, from the knowledge of deposition time and flux measurements, we estimate that the thickness of the QDs grown during three deposition cycles is about 1-2 MLs.

The cw and time-resolved PL (TRPL) measurements were performed by placing the sample at the cold stage of an Advanced Research Systems (ARS) closed cycle refrigerating system at different temperatures. For cw-PL measurements, the 351 nm line from an Ar⁺ laser was used for excitation. The PL emission was detected by a TriVista SP2 500i Triple monochromator coupled to a thermoelectrically cooled GaAs photomultiplier tube (PMT) and a photon counting system. The TRPL studies were performed using the 337 nm line of a Newport N₂ pulsed laser with 4 ns pulse width. The signal was recorded using a 500 MHz Tektronix TDS 654C oscilloscope. The excitation intensity was varied over five orders of magnitude using neutral density filters (NDFs).

The HRXRD measurements were carried out at Beamline X20A at the National Synchrotron Light Source (NSLS) at the Brookhaven National Laboratory (BNL). All measurements were performed using monochromatic synchrotron radiation at 8 keV ($\lambda = 1.54056 \text{ \AA}$), with a double-crystal Ge (111) monochromator. The incident beam size was set to about $1 \times 1.5 \text{ mm}^2$. The diffracted beam path consisted of scatter slits, followed by a Ge (111) analyzer in front of the detector. ω - 2θ scans for symmetric (004) and (002) reflections were measured. For reciprocal space map measurements, a series of ω - 2θ scans, each offset by $\delta\omega = 0.04^\circ$ were performed.

III. RESULTS AND DISCUSSION

A. Formation of stacked QDs

HRXRD based RSMs have been used to observe vertical and lateral correlations, diffuse scattering due to strain fluctuations, and lateral peak broadening of the superlattice and multilayer structures containing quantum dots.^{18–22} The RSM of the ZnMgTe/ZnSe multilayer structure consists of

periodic superlattice peaks in the q_x direction arising from a finite correlation length of the multilayer structure as shown in Fig. 2 for (002) reflection. Here, the peak labeled S(002) corresponds to the diffraction from the substrate, and SL(n) is the n -th superlattice peak of the multilayer structure with the spacing between the satellite peaks given by $2\pi/D$, where D is the superlattice period and n is an integer. The spacing between the SL(0) and the substrate peak is proportional to the relative difference of the vertical lattice constant of the substrate and the averaged lattice constant of the multilayer structure.

The ZnMgTe QDs embedded in a ZnSe matrix give rise to diffuse scattering accompanying the coherent diffraction from the whole multilayer structure. The diffuse scattering is caused by the difference in the scattering factors of ZnMgTe and ZnSe and the elastic deformation strain field in the ZnSe matrix surrounding the dots. A theoretical description of the x-ray scattering from the QD arrays based on a statistical kinematical approach¹⁸ showed that if the dots are fully correlated vertically, and if we neglect the surface stress relaxation, the q_z dependence of the scattered intensity is mainly determined by the structure factor of the multilayer structure. Thus, in RSM, the diffuse scattered intensity is concentrated in “stripes” parallel to the q_x axis at the same positions $q_z = 2\pi n/D$ as the coherent superlattice maxima. On the other hand, if the dots are completely uncorrelated vertically, the scattered intensity is rather broad and exhibits no stripe-like structure.¹⁸ As observed for the ZnMgTe/ZnSe multilayer structures shown in Fig. 2, the diffuse scattered intensity is elongated along the q_x direction. Such an elongation of the diffraction maxima in the q_x direction can be due to (i) shape of individual dots; this is less likely in our sample because elongation in the q_x direction would mean that the dots have the form of vertical needles, which is not true in our case, (ii) strain field around the dots; we excluded this possibility by comparing the RSM taken in (004) direction. The displacement field $\mathbf{u}(\mathbf{r})$ enters the formula for the diffracted intensity in the dot product $\mathbf{h} \cdot \mathbf{u}$ with the reciprocal-lattice vector \mathbf{h} . Therefore, the strain broadening of the (004) maximum should be approximately two times larger than in (002). Preliminary measurements on the RSM around SL(-1) peak for (004) reflection showed that the broadening in the q_x direction is about the same as observed for (002) reflection ($\sim 0.042 \text{ \AA}^{-1}$), (iii) vertical correlation of the dots; the correlation in the dot positions enters the correlation function of the local electron density, which does not depend on \mathbf{h} . Hence, we concluded that the elongation of the diffuse scattered intensity in the q_x direction indicates a vertical correlation of the dots in the investigated multilayer structure.

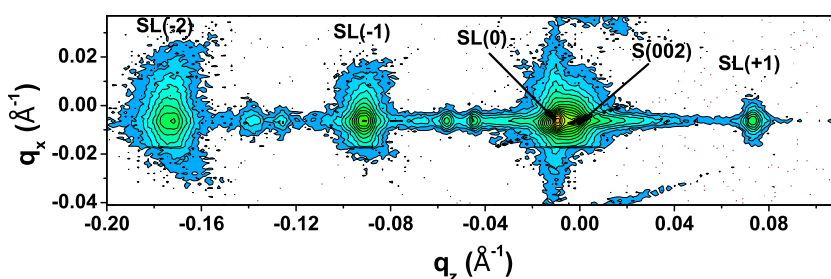


FIG. 2. The reciprocal space map for (002) reflection of the ZnMgTe/ZnSe multilayer structure with one hundred periods showing elongation of diffuse scattered intensity along q_x direction.

Hence, an array of stacked ZnMgTe/ZnSe QDs of different sizes is formed within the studied multilayer structure. The ordering of QD in the growth directions was proposed previously to explain strong Aharonov-Bohm oscillations in similar ZnTe/ZnSe type-II QDs.^{16,23}

A low energy-shift and decreased FWHM in PL of stacked QDs have been previously observed with the evidence of formation of coherent superlattice-like states.²⁴ At this point, we cannot comment if incorporation of Mg plays any role in increasing or decreasing correlation of the QDs compared to previously studied samples without Mg^{4,5,25} mainly because of the different growth conditions and compositions of the samples. However, we found that the addition of Mg in the QD layers contributed to the higher x-ray scattering intensity of the SL peaks.¹⁷ For ZnMgTe/ZnSe, we observed SL peaks up to fifth order compared to the ZnTe/ZnSe case,^{4,25} where we could resolve SL peaks only up to second order.

B. Excitation dependent photoluminescence

The PL spectra for ZnMgTe/ZnSe multilayer structure are shown in Fig. 3 for three different excitation intensities obtained at $T = 7$ K. The PL spectrum is a broad band centered at 2.35 eV at maximum excitation intensity at 7 K. The spectrally broad luminescence is caused by fluctuations in dots size and composition, hence distribution of the density of states over a wide energy range, as well as due to a strong electron-phonon coupling, as discussed below. In Sec. III A we have shown that these dots are vertically correlated along the growth direction. We note that, for $0.1I_{max}$ (I_{max} is the maximum excitation intensity in our cw-PL experiment), the lower energy side of the PL band does not shift from its position at the maximum excitation intensity, while for $0.001I_{max}$, the higher energy side of the band shows significant red-shift compared to the lower energy side of the band as shown in inset of Fig. 3. For a detailed investigation of the behavior of the PL band at different positions under varying excitation intensities, we have plotted the peak positions of (a) 80% of

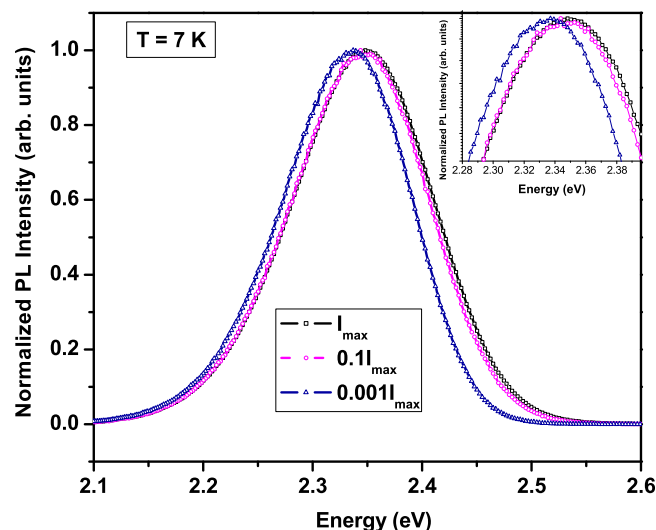


FIG. 3. PL spectra for ZnMgTe/ZnSe multilayer structure measured for three different excitation intensities at 7 K.

the maximum luminescence intensity at the LES of the band, (b) maximum luminescence intensity near the center of the energy band (CEB), and (c) 80% of the maximum luminescence intensity at the HES of the band as a function of the excitation intensity for over five orders of magnitude in Figs. 4(a)–4(c), respectively. The peak positions of LES, CEB, and HES show a blue shift of approximately 12, 21, and 25 meV, respectively, with increasing excitation intensity. In general, such a strong blue shift with increasing excitation intensity is a hallmark of type-II nanostructures,^{5,26,27} caused by narrowing of the triangular quantum well formed at the QD-barrier interface due to spatial separation of the photogenerated carriers. In our case, electrons are located within the ZnSe, while holes are confined in ZnMgTe. The different magnitudes of blue-shifts corresponding to different positions of the PL band can be explained by the size distribution of the ZnMgTe QDs formed within the structure. The contribution from the larger size dots dominates at the lower energy side of the band, whereas the contribution from the smaller size dots is dominant at the higher energy side of the band. Larger dots have more closely spaced energy levels compared to the smaller dots, hence the relative change in energy levels for the carrier is smaller for larger dots. As a result, the larger dots will show a smaller blue-shift²⁸ as compared to that of smaller dots under equal change in excitation intensity as seen in Fig. 4.

For the intermediate excitation intensities, the peak positions of LES and CEB follow the cube root of excitation

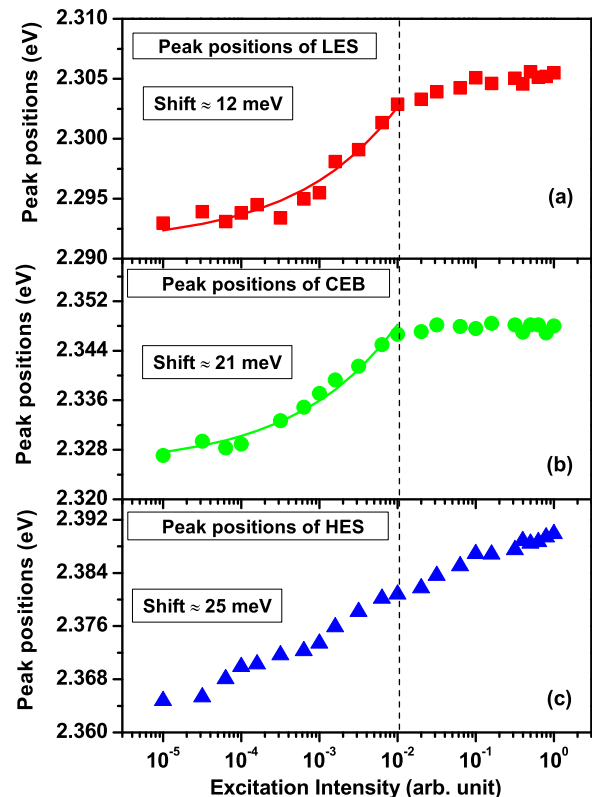


FIG. 4. The peak positions as a function of excitation intensity determined at energies for (a) 80% of the maximum PL intensity at the LES of the band; (b) maximum PL intensity near the CEB; (c) 80% of the maximum PL intensity at the HES of the band. The solid lines in (a) and (b) are cube root dependence of the excitation intensity.

intensity as predicted for type-II quantum structures,^{5,26,27,29} shown by the solid lines in Figs. 4(a) and 4(b), respectively. The Coulomb interaction of the photo-generated carriers leads to the band bending and formation of a quantum well at the ZnMgTe-ZnSe interface at intermediate excitation intensities. For highest excitation intensities, band-bending saturates and, as a result, the peak position does not shift much with increasing excitation intensity.

The behavior of the excitation intensity dependent peak position of HES does not follow the cube root of the excitation intensity as shown in Fig. 4(c). This peak position shifts faster towards higher energies with increasing excitation intensity because of increased contribution of the emission from Te_n IBEs; these centers located in the barriers, arise from a small fraction of Te (<1%) in the barriers, as discussed above (see also Ref. 15). Similar effects of IBE have also been observed in magneto-PL,¹⁶ where effects associated with type-II QDs were observed only at relatively low excitation intensities, whereas at high excitations they were masked by IBE emission.

C. Time resolved photoluminescence

The normalized TRPL spectra of ZnMgTe/ZnSe multi-layer QD structure are shown in the insets of Figs. 5(a) and 5(b) for the 2.3 and 2.4 eV detection energies (taken at approximately 80% of the maximum PL intensity at the lower and higher energy sides of the emission band) for four different excitation intensities at $T = 7$ K. The PL decay time

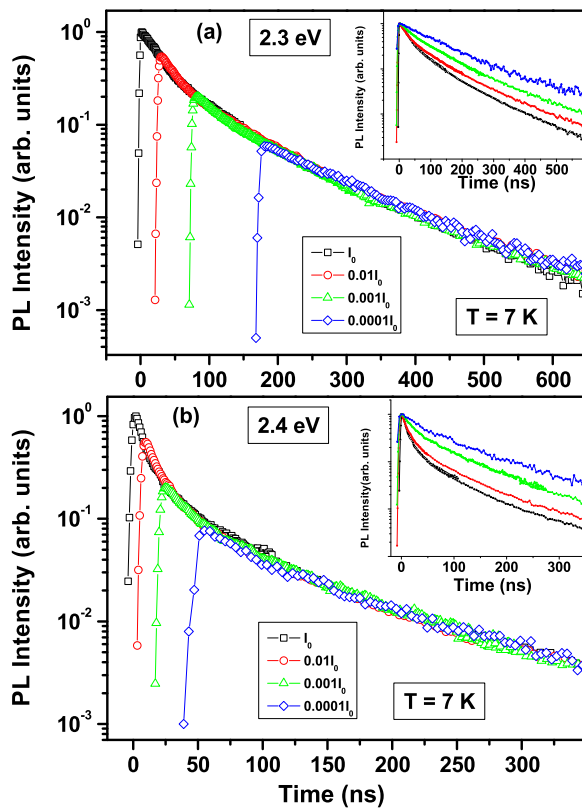


FIG. 5. The behavior of decay time decay at detection energies (a) 2.3 eV and (b) 2.4 eV (energies at approximately 80% of the peak position of the maximum PL intensity in the lower and higher energy sides of the PL band), for four different excitation intensities.

at higher excitation intensity shows a non-exponential decay with a fast decay at initial observation times and approaches a single exponential decay at longer observation times. Also, as the excitation intensity decreases, the PL decay time approaches a single exponential decay with a well-defined decay time. At higher excitation intensity at $t = 0$, a larger carrier concentration of the photogenerated electron-hole pairs results in band bending, hence a stronger overlap of electron-hole wave-functions, and thus a faster decay. However, as time passes and at a later instance $t = t_1$, the carrier concentration decreases. As a result, the band-bending effects become negligible which lead to a weaker overlap of the wave-functions and a single exponential decay with a well-defined decay time. Such behaviors of decay time under various excitation intensities are regularly observed in type-II nanostructures.^{5,26,27,29} The carrier concentration at higher excitation intensity at, say $t = t_1$ is equal to the initial carrier concentration at $t = 0$ for lower excitation intensity. Therefore, by simply shifting the point $t = 0$ of lower the excitation intensity to $t = t_1$ of the higher excitation intensity, the respective lower excitation intensity curve must coincide with the part of the higher excitation intensity curve for $t > t_1$. The curves at different excitation intensities shown in inset of Figs. 5(a) and 5(b) have been rescaled by shifting the observation times and plotted as a master curve in Figs. 5(a) and 5(b) for detection energies 2.3 eV and 2.4 eV, respectively. One can see that the time decays from all three different excitation intensities form a single decay after shifting the observation times. The excitation intensity dependent behavior for ZnMgTe/ZnSe QDs confirms the existence type-II band alignment in the studied sample.

Fig. 6(a) shows the behavior of the decay time at an intermediate excitation intensity of $0.001I_0$ (I_0 is the maximum excitation intensity of our TRPL experiment) for three different detection energies of the PL band at 2.3, 2.35, and 2.4 eV. The PL decay shows an exponential behavior at detection energies of 2.3 eV and 2.35 eV for such intermediate excitation intensities but for detection energy of 2.4 eV, the decay continues to show a non-exponential behavior. However, to compare the PL decay time across the whole spectrum, we have obtained a characteristics decay time (τ_c) as a function of detection energy for $0.001I_0$ excitation intensity, which we plot in Fig. 6(b), along with the observed PL band. We found $\tau_c \sim 129$ ns at 2.18 eV; it decreases slowly with increasing detection energy, until it reaches the value of $\tau_c \sim 112$ ns at 2.35 eV. After that, there is a monotonically sharp decrease in τ_c with increasing detection energy up to 2.53 eV, for which $\tau_c \sim 19$ ns. Such a large value of τ_c (~ 129 ns) at the detection energies at the lower energy side of the band is explained by a relatively weak overlap of the electron and hole wave functions of the spatially separated carriers at the ZnMgTe-ZnSe interface due to type-II band alignment. The PL at 2.18 eV is dominated by the large QDs; with increasing detection energy up to 2.35 eV, the contribution from the smaller dots gradually increases. For smaller dots, the overlap of the electron hole wave functions is stronger, hence τ_c is found to decrease, albeit slowly, with increasing detection energy up to 2.35 eV. At higher energy, the contribution from IBEs starts to increase and ultimately

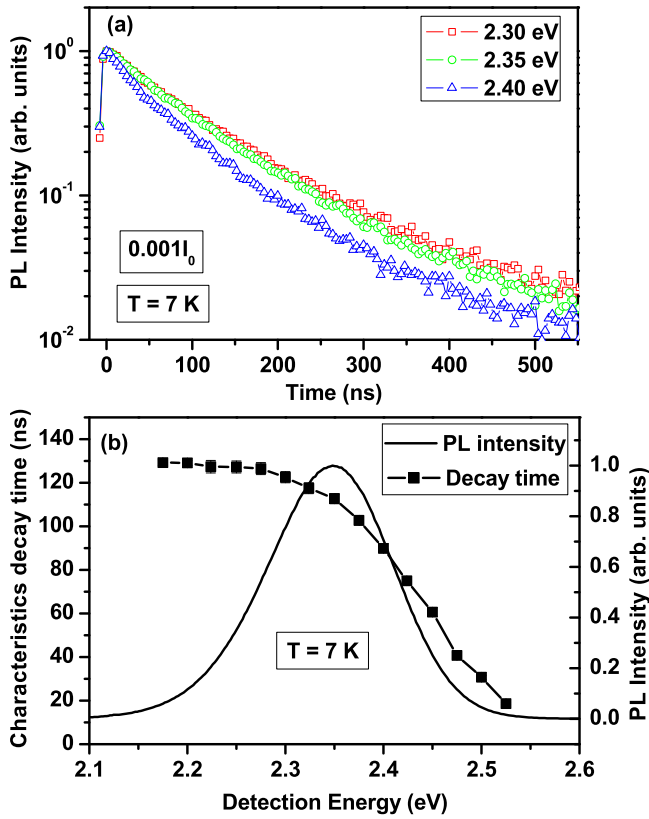


FIG. 6. (a) The behavior of decay time at an intermediate excitation intensity for three different detection energies of the PL band at 2.3 eV, 2.35 eV, and 2.4 eV. (b) The dependence of characteristics decay time (τ_c) on the detection energy.

dominate; as a result, there is a sharp decrease in τ_c with increasing detection energy. Such a behavior of PL life-time decay has been reported for a smooth transition of the PL from the blue band of IBEs of Te atoms to the green band of type-II ZnTe/ZnSe QDs.^{30,31} However, the spectral dependent values of the decay time for ZnMgTe/ZnSe structures are much higher ($\tau_{max} \sim 129$ ns at lower energy side) than that of ZnTe/ZnSe case ($\tau_{max} \sim 80$ ns at lower energy side³⁰). We suggest that this could be due to the formation of larger dots with incorporation of Mg and larger content of Te.

We mentioned above that the time decay continues to show a non-exponential behavior even at $0.001I_0$ excitation intensity at detection energy of 2.4 eV. At the higher energy side of the band at 2.4 eV, the contribution from IEBs starts to dominate; hence, there is a stronger overlap between the electron and hole wave functions even at intermediate excitation intensity. As a result, the time decay is faster at initial observation times even at an intermediate excitation intensity showing a non-exponential behavior at $0.001I_0$ excitation intensity at 2.4 eV.

D. Temperature dependent photoluminescence

The temperature dependence of the peak position and FWHM as a function of temperature, and integrated PL intensity as a function of inverse temperature of the broad PL band are shown in Figs. 7(a)–7(c), respectively, for two different excitation intensities. We found that the peak

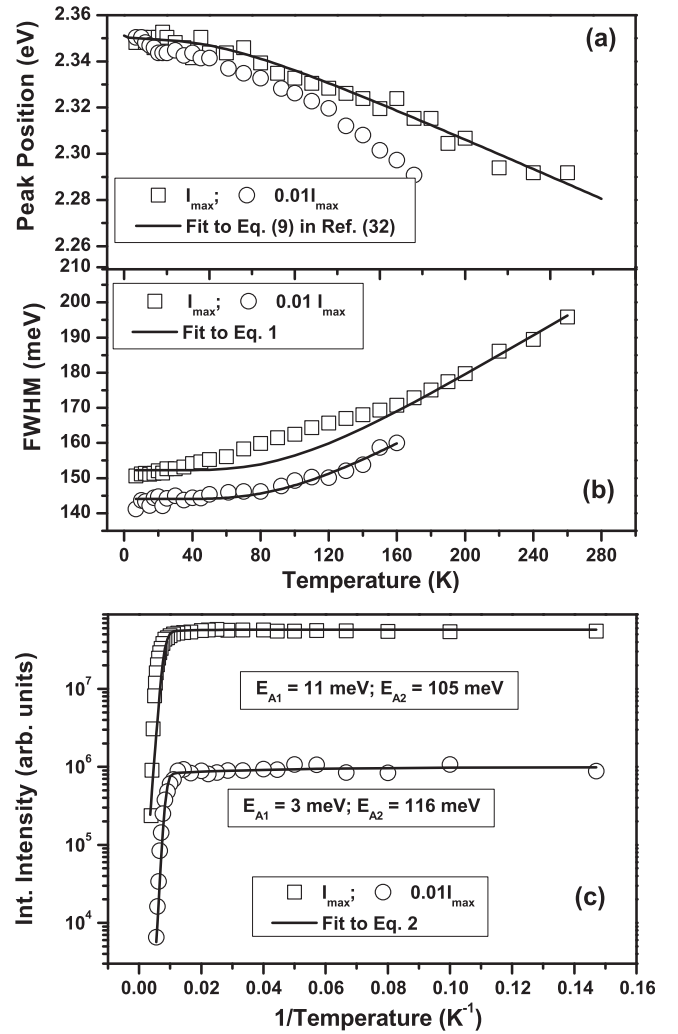


FIG. 7. The temperature dependence of the (a) peak position, (b) FWHM, and (c) integrated PL intensity of the PL band for two different excitation intensities. The solid line in (a) is fit to the temperature dependent bandgap of ZnTe plotted by shifting to the value of ZnMgTe in the energy axis. The solid lines in (b) and (c) are fits to Eqs. (1) and (2), respectively.

position undergoes a red-shift of approximately 65 meV with increasing temperature up to 280 K for maximum excitation intensity. It is generally accepted that the modification of the bandgap is caused by the cumulative effects of thermal lattice expansion and electron phonon-interaction. For comparison, we have plotted the temperature dependent bandgap of ZnTe calculated based on a four parameter semi-empirical model introduced by Passler^{32,33} by shifting it to the value of ZnMgTe in the energy axis. We can see that the temperature dependent bandgap of the ZnMgTe QDs follows very closely the bandgap of ZnTe for maximum excitation intensity as shown in Fig. 7(a). However, for $0.01I_{max}$, the temperature dependent bandgap does not follow the bandgap of ZnTe, where the emission is shifted more towards lower energy above 50 K. In the case of emission arising from a “collection” of centers with different energies, such as sets of QDs and/or various isoelectronic centers, as in our case, such a behavior is expected due to ionization (quenching) of the centers with lower activation energy. At this point, some of the carriers may redistribute to the deeper centers further shifting emission

to the lower energy [see, e.g., Ref. 5 and references therein], as a result, the emission becomes dominated by relatively deeper centers.

We note that the FWHM increases with increasing temperature even at lower temperature, which is in contrast to the band narrowing with increasing temperature, typical of an ensemble of QDs, resulting from the enhanced carrier relaxation process related to the size distribution of QDs,^{34,35} can be attributed to the electron-phonon scattering.^{36–39} For strong electron-phonon coupling, in the Gaussian approximation, the temperature dependence of the FWHM can be described as^{38,39}

$$FWHM(T) = [(8 \ln 2)S(\hbar\omega)^2(2n + 1)]^{1/2}, \quad (1)$$

where $n = [\exp(\hbar\omega/kT) - 1]^{-1}$, k is the Boltzmann constant, S is the Huang-Rhys factor, determining the coupling strength, and $\hbar\omega$ is the phonon energy. From the fit of Eq. (1) to the temperature dependent FWHM as shown in Fig. 7(b), we obtain $S \sim 4.30 \pm 0.17$ and $\hbar\omega \sim 31.6 \pm 0.7$ meV. Remarkably, the phonon energy nearly equals to that of ZnSe LO phonon energy (31.8 meV⁴⁰). This indicates that strong electron-phonon coupling along with the size and composition fluctuation of the dots is responsible for broadening of the PL. However, we find that Eq. (1) does not fit well to the data

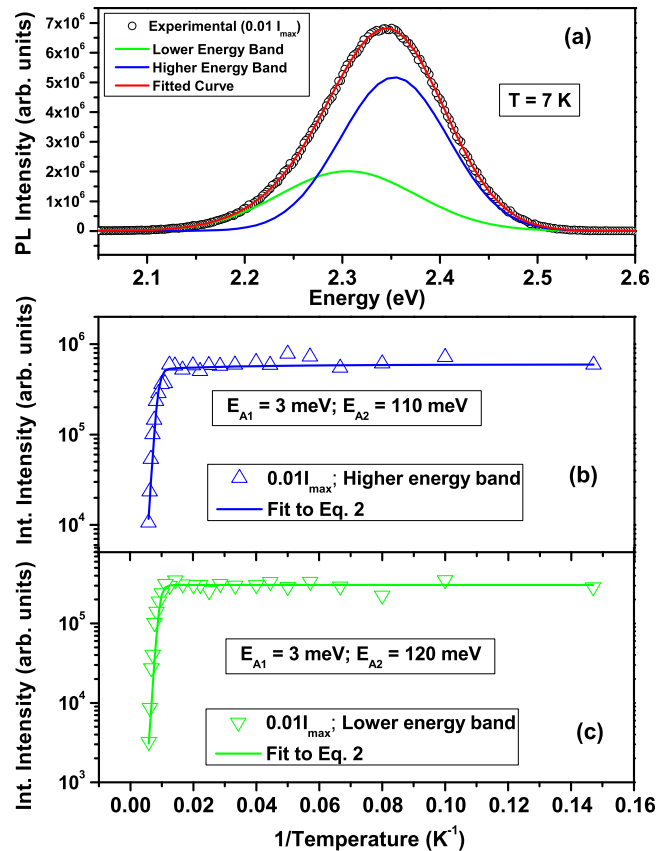


FIG. 8. (a) The broad PL band for $0.01I_{\max}$ excitation intensity is decomposed into two Gaussians. Integrated PL intensity of the lower and higher energy bands as a function of inverse temperature is shown in (b) and (c), respectively, determined by decomposing the broad PL band into two bands as shown in (a). The solid lines in (b) and (c) are fits to the dual activation energy model described in Eq. (2).

obtained at maximum excitation intensity at $T < 160$ K as shown in Fig. 7(b). At $T < 50$ K, the contribution from LO phonon-electron interaction is expected to be less significant, and the FWHM is determined by the competition between the LO phonon-electron interaction, increasing FWHM, and enhanced carrier ionization/relaxation process in the QDs, which results in effective decrease in FWHM. For maximum excitation intensity, the contribution from IBEs is relatively higher, and because of a strong LO phonon-electron coupling for IBEs, there is a faster increase in FWHM with increasing temperature at $50 \text{ K} < T < 160 \text{ K}$. At $T > 160$ K, the FWHM is mainly determined by the LO phonon electron coupling for the QDs.

The integrated PL intensity almost stays constant up to 100 K and then starts to decrease with increasing temperature up to 280 K for maximum excitation intensity. The temperature dependent quenching of PL intensity is caused by thermal escape of charge carriers from confined QD states into the barriers followed by non-radiative recombination.^{41–43} To calculate the values of the activation energies required for the carriers to escape from the QD states into the barrier, we have plotted the integrated PL intensity for two different excitation intensities as function of inverse temperature in Fig. 7(c). The temperature dependent integrated PL intensity cannot be fitted by an Arrhenius plot using single thermal activation but can be fitted quite well in the entire temperature range using a dual activation energy model,^{43,44} given by

$$I_{\text{int}}(T) = \frac{I_{\max}^0}{\left[1 + \left(C_1 e^{-\frac{E_{A1}}{kT}} + C_2 e^{-\frac{E_{A2}}{kT}}\right)\right]}. \quad (2)$$

The result of the fitting is shown by the solid lines in Fig. 7(c) for two different excitation intensities. The parameters C_1 and C_2 represent the relative ratios of the non-radiative recombination and reflect the competitive relation between the recapture and non-radiative recombination. I_{\max}^0 is the maximum integrated PL intensity. The E_{A1} and E_{A2} are the activation energies of two different thermal activation processes. The values of E_{A1} and E_{A2} are found to be 3 and 116 meV for an intermediate excitation intensity of $0.01I_{\max}$ (small band bending), respectively.

We attribute the activation energy, $E_{A1} \sim 3$ meV to the type-II exciton binding energy; therefore, it represents thermal escape of electrons away from QD, breaking the type-II exciton. The value of $E_{A1} \sim 3$ meV is significantly lower than the free exciton binding energy of either ZnSe⁴⁵ (~ 20 meV) or ZnTe⁴⁵ (~ 13 meV) but in the range of the values previously reported for ZnTe/ZnSe type-II QDs.^{5,46,47} We attribute the activation energy, $E_{A2} \sim 116$ meV to the ionization of the holes, which thermally escapes after making a transition from the QD ground state to the barrier. The activation energy, $E_{A2} \sim 116$ meV is smaller compared to 178 meV reported for ZnTe/ZnSe QD;¹⁵ this is expected because of lowering of the valence band offset with introduction of Mg (see detailed discussion in Sec. III E). For maximum excitation intensity I_{\max} , the band bending results in a higher value of activation energy corresponding to ionization

of the electrons (as high as $E_{A1} \sim 11$ meV) and a lower value of activation energy corresponding to ionization of the holes ($E_{A2} \sim 105$ meV). We also note that for the maximum excitation intensity, the dual activation energy model described in Eq. (2) does not fit well to the temperature dependent integrated PL intensity in the range $50 \text{ K} < T < 160 \text{ K}$ because of a contribution from the faster ionization of the IBEs, which also leads to a faster increase in FWHM with increasing temperature as described above.

To investigate the dependence of activation energies on the size fluctuation of the dots, we have decomposed the broad PL band for $0.01I_{max}$ excitation intensity into two Gaussian bands as shown in Fig. 8(a) and plotted the integrated PL intensity of the higher and lower energy bands as a function of inverse temperature in Figs. 8(b) and 8(c), respectively. Note that the PL band at higher energy side contains the high energy tail contribution from larger dots; similarly, PL band at lower energy side contains near band edge emissions from small dots. However, the contribution from the smaller sizes of the dots dominates at higher energy side of the band, and the contribution of larger sizes of the dots dominates at lower energy side of the band as determined earlier by excitation intensity dependent PL peak positions at higher and lower energy side of the band (Fig. 4). The solid lines in Figs. 8(b) and 8(c) are fits to the dual activation energy model described in Eq. (2) for the higher and lower energy bands, respectively. We found that the activation energy, E_{A2} corresponding to the ionization of holes is approximately 120 meV for the lower energy side of the band, where emission is dominated from larger size of the dots dominates. The E_{A2} becomes 110 meV for the higher energy side of the band, where the emission is dominated by the smaller size of the dots.

The PL decay time is also found to decrease with increasing temperature caused by the thermal escape of charge carriers from confined QD states into barrier followed by non-radiative recombination.^{41,42,48} To compare the values of the activation energies as deduced from the temperature dependent PL intensity, we have plotted τ_c as a function of temperature for 2.35 eV for an intermediate excitation intensity in Fig. 9. The behavior of temperature dependent on the characteristic decay time, τ_c can be fitted to the following expression:^{5,46,49}

$$\tau_c = [(\tau_r/(1 - Ce^{-E_{A1}/kT}))^{-1} + (\tau_{nr}e^{E_{A2}/kT})^{-1}]^{-1}, \quad (3)$$

for the whole temperature range as shown by solid line in Fig. 9. Here, τ_r is the radiative decay time at $T = 0 \text{ K}$, τ_{nr} is the non-radiative decay time, and C is a constant. The values of τ_r and τ_{nr} are found to be approximately 112 and 0.15 ns, respectively. As seen in Fig. 9, τ_c increases with the increasing temperature up to 90 K. As the temperature rises, the weakly bound electrons are ionized, and as a result, are away from the strongly localized holes for an increasing fraction of their lifetimes, which in turn lengthens the PL decay time. We note that such an explanation is valid provided that the non-radiative processes are negligible, which is confirmed by almost constant PL intensity in the same temperature region as shown in Fig. 7(c). The values of the E_{A1} and E_{A2}

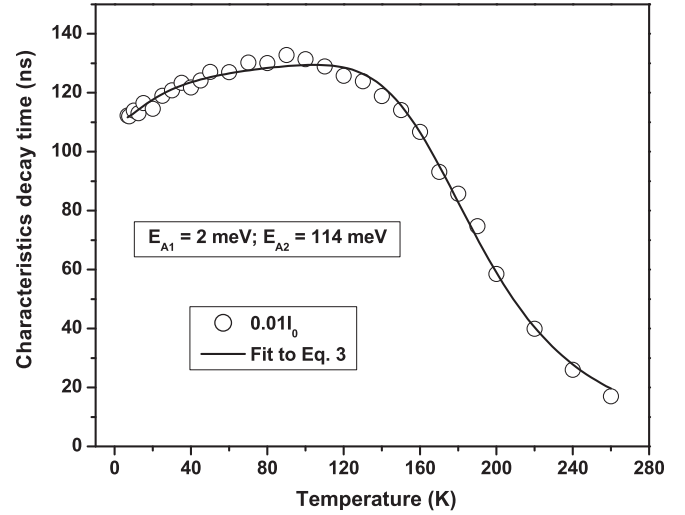


FIG. 9. The temperature dependence of the characteristic decay time for an intermediate excitation intensity for 2.35 eV. The solid line is fit to Eq. (3).

are 3 and 114 meV, respectively, for intermediate excitation intensity, which is an excellent agreement with the values as deduced from fitting of Eq. (2) to the temperature dependent integrated PL intensity for similar excitation.

E. Estimation of bandgaps and QD energy levels

To estimate the values of the bandgaps and QD energy levels, we have determined the compositions of the constituent elements of the ZnMgTe/ZnSe multilayer structure by the HRXRD measurement and solved the 1-D Schrodinger's equation for a square well potential. The experimental ω - 2θ curves showed that a set of subsidiary satellite peaks up to fifth order arises from interference between each of the layers symmetrically around the SL(0) peak for both the (004) and (002) reflections for ZnMgTe/ZnSe multilayer structures.¹⁷ To extract structural parameters of the multilayer structure, the ω - 2θ curves were simulated by the commercially available BEDE RADS program after an estimation of the initial fitting parameters.^{17,25} For simulation purposes, we replaced the QD array by an effective layer, whose scattering factor is an average of the scattering factors of the dots and the crystal matrix. The simulation result showed that the average thicknesses of the ZnMgTe layer containing QDs and ZnSe barrier are about 0.1 and 3.6 nm, respectively.¹⁷ The simulation result also showed that while most of Te is confined inside the QD-containing layer, there is a small amount of Te ($\sim 1\%$) diffusion inside the barrier. It is also found that there is approximately 30% Mg within the ZnMgTe layer.¹⁷

Having estimated Mg concentration ($x = 0.30$), we calculate the band-gap of the $Zn_{1-x}Mg_xTe$ QD, $E_{g,ZnMgTe}$, from the following equation:

$$E_{g,ZnMgTe} = E_{g,ZnTe}(1-x) + E_{g,MgTe}x - b_{ZnMgTe}(1-x)x, \quad (4)$$

where $E_{g,ZnTe}$ and $E_{g,MgTe}$ are band gaps of ZnTe and MgTe, respectively, and b_{ZnMgTe} is the bowing parameter. Similarly, the band-gap of the $ZnTe_xSe_{1-x}$ barrier for Te composition of 1% is also evaluated. Fig. 10(a) shows the band diagram

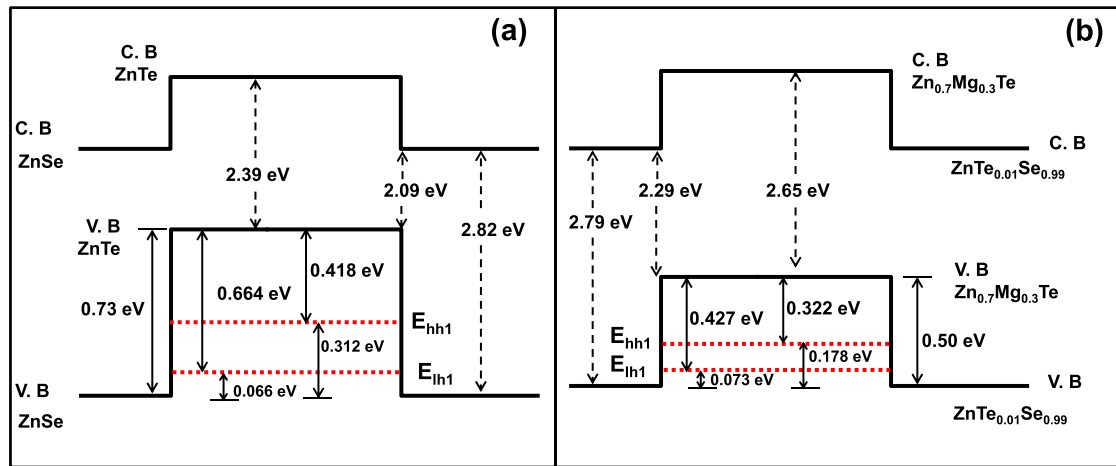


FIG. 10. Estimated band-gaps, band offsets, and hole energy levels of the (a) ZnTe/ZnSe and (b) ZnMgTe/ZnSe multilayer structure. Incorporation of Mg modifies the ZnTe bandgap, valence band-offset, and hole activation energy without changing the ZnSe barrier bandgap in any significant manner.

of an ideal ZnTe/ZnSe structure, while Fig. 10(b) shows the estimated band-gaps and resulting valence band and conduction band offsets of the studied ZnMgTe/ZnSe multilayer system with an estimated Mg concentration of 30% inside the QDs and 1% Te inside ZnSe barrier. Specifically note that the VBO between ZnMgTe QDs and ZnSeTe barrier is determined to be about 0.50 eV on assuming the VBO between ZnTe and ZnSe is 0.73 eV,¹² which decreases linearly with increasing Mg composition.¹⁰ The VBOs and the bandgaps were obtained by assuming the bandgaps of ZnSe, ZnTe, and MgTe are 2.82, 2.39, and 3.67 eV, respectively.⁵⁰ The bowing parameters b_{ZnMgTe} and b_{ZnTeSe} are taken to be 0.67 and 1.20 eV,⁵¹ respectively. From the comparison of the bandgaps and band offsets of ZnTe/ZnSe system and ZnMgTe/ZnSe system as shown in Figs. 10(a) and 10(b), respectively, we see that we can fine control of the ZnTe QD bandgap and valence band-offset without changing the ZnSe barrier bandgap in any significant manner. Hence, we can effectively tune the optical properties of ZnSe by incorporating Mg inside the ZnTe QDs.

The carrier confinement in type-II systems, such as ZnTe/ZnSe, is independent of the bandgaps of the underlying materials but rather depends on the band offsets. From the conditions of growth, we estimate that the thickness (height, h) of ZnMgTe QDs varies from 1 to 2 MLs, and the confinement energy mainly comes from the confinement of the carriers along the growth direction. Taking $h = 0.5$ nm, as an average dot thickness, the heavy- and light-hole energy levels along the growth direction are evaluated simply by solving 1-D Schrodinger's equation for a square well potential of 0.50 eV for ZnMgTe QDs. The solution gives two hole energy levels, E_{hh1} at 322 meV (ground state heavy hole) and E_{lh1} at 427 meV (ground state light hole) as shown in Fig. 10(b) for ZnMgTe QDs. Note that the additional confinement due to finite size in x - y plane is negligible due to a presumed large diameter of QDs, which is in the order of ~ 20 nm.¹⁶ Assuming the holes thermally escape after making transitions: (i) from the QD heavy-hole ground state (E_{hh1}) to the barrier, and (ii) QD light-hole ground state (E_{lh1}) to the barrier with the increasing temperature, the activation energies are determined to be 178 meV for heavy hole transitions ($E_{\text{A2, hh}} \sim 178$ meV)

and 73 meV for light hole transitions ($E_{\text{A2, lh}} \sim 73$ meV). The reported values of $E_{\text{A2}} \sim 114$ – 116 meV have been obtained from thermal quenching of the integrated PL, which includes all possible transitions; therefore, this value has to be compared with the average activation energy ($E_{\text{A2, av}} \sim 125$ meV) corresponding to the heavy- and light-hole transitions to the barrier. This “average” value would also change with temperature due to changing population of light and heavy holes levels; however, it seems qualitatively match the experimentally observed values. Hence, the activation energy corresponding to the ionization of holes is determined by competing heavy- and light-hole transitions to the barrier. On the other hand, ZnTe/ZnSe QDs with thickness of 0.5 nm and the valence band offset of 0.73 eV give rise to heavy- and light-hole energy levels, E_{hh1} at 418 meV and E_{lh1} at 664 meV corresponding to the activation of heavy holes $E_{\text{A2, hh}} \sim 312$ meV and light holes $E_{\text{A2, lh}} \sim 66$ meV leading to an average activation energy $E_{\text{A2, av}} \sim 190$ meV as shown in Fig. 10(a). Hence, incorporation on 30% Mg inside the ZnTe QDs reduces the hole activation energy by approximately 65 meV. As a result, the probability of finding free holes is enhanced, and indeed a hole free carrier concentration in the order of $\text{mid-}10^{15} \text{ cm}^{-3}$ has been observed¹³ for the first time, in such samples.

The calculated modified band diagram for the ZnMgTe/ZnSe QDs will give us a PL spectrum with peak position at around 2.61 eV, whereas the experimentally observed PL peak position is at around 2.35 eV. Such a large shift in PL peak position is due to a large Frank-Condon shift owing to a strong electron-phonon coupling. The Frank-Condon shift ($S\hbar\omega$) is approximately 136 meV for $S = 4.3$ and $\hbar\omega = 31.6$ meV as determined by the temperature dependent FWHM for ZnMgTe QDs, giving theoretical value for the PL band centered around 2.47 eV, which is within errors of our estimations (we note that shifts as large as 240 meV for ZnTe/ZnSe systems have been previously reported³⁸), and moreover the size and composition distributions also contribute to the broadening and shift to a lower energies.

We propose that engineering the bandgaps and valence band-offsets with incorporation of Mg in ZnTe/ZnSe systems without modifying the barrier bandgap will also allow us to create and control the QD intermediate band lying within the

ZnSe (or related alloys) forbidden energy gap, which may absorb photons with energies below the barrier bandgap, with potential application in solar cells. The below bandgap photon absorption is expected to increase the short circuit current, while preserving the open circuit voltage of an intermediate band solar cell.¹⁴ In type-II system, such as ZnMgTe/ZnSe, where the intermediate band is engineered out of hole confinement energy also has the advantage of relatively large carrier life-time while suppressing non-radiative Auger recombination.

IV. SUMMARY

In summary, submonolayer quantities of Mg are introduced in multilayer ZnMgTe/ZnSe QD structure to modify the bandgaps and the valence band offset of ZnTe relative to ZnSe. The ZnMgTe dots are found to be correlated along the grown direction forming an array of stacked QDs with the photoluminescence emission showing a broad band caused by the size and composition fluctuation of the dots. The higher (lower) energy side of the band, where the contribution from smaller (larger) size of the dots is dominant, shows a larger (smaller) blue-shift with increasing excitation intensity because of a higher (lower) carrier density produced by the smaller (larger) dots. The IBEs also contribute at the higher energy side of the band with an apparent shift of the peak position towards higher energies resulting in a non-cube root dependence on excitation intensity. The characteristics decay time of the carriers show a weaker dependence on the size fluctuation of the dots (~ 129 ns), which however decreases sharply with an increase in contribution from IBEs because of a stronger overlap of the electron-hole wave functions. At lower temperature, the FWHM of the PL band is determined by the competition between the LO phonon-electron interaction and enhanced carrier relaxation process of the QDs. With increasing temperature, the IBEs with stronger electron-phonon coupling shows a faster increase in FWHM and after that the FWHM is mainly determined by ionization of carriers within the QDs. Analysis of the temperature dependent PL intensity and decay time reveals that two thermally activated processes, ionization of electrons from QDs to the barrier by breaking the type-II excitons, and ionization of holes which thermally escape after making a transition from the hole ground state to the barrier are responsible for PL intensity quenching and decrease in decay time with increasing temperature. The activation energy corresponding to the ionization of holes is also found to be dependent on the size of the dots.

Incorporation of Mg in ZnTe QDs modifies the QD bandgap, and reduces the hole activation energy by approximately 65 meV, which is responsible for previously observed free hole carrier concentration in ZnMgTe/ZnSe system. Engineering the hole confinement level by incorporating Mg may also help to absorb photon energies below the barrier semiconductor bandgap, while suppressing non-radiative Auger recombination.

ACKNOWLEDGMENTS

This research was supported by the U.S. Department of Energy, Office of Basic Energy Sciences, Division of

Materials Sciences and Engineering under Award No. DE-FG02-10ER46678. Use of the National Synchrotron Light Source, Brookhaven National Laboratory, was supported by the U.S. Department of Energy, Office of Science, Office of Basic Energy Sciences, under Contract No. DE-AC02-98CH10886. We thank J. Jordan-Sweet, B. Roy, R. Moug, L. Li, and M. Treger for assistance during the experiments and useful discussion. We also thank V. Holy for discussion in interpreting the RSM.

- ¹M. P. Mikhailova and A. N. Titkov, *Semicond. Sci. Technol.* **9**, 1279 (1994).
- ²C. Weisbuch and B. Vinter, *Quantum Semiconductor Structures: Fundamentals and Applications* (Academic, CA, 1991).
- ³V. I. Klimov, S. A. Ivanov, J. Nanda, M. Achermann, I. Bezel, J. A. McGuire, and A. Piryatinski, *Nature* **447**, 441 (2007).
- ⁴Y. Gong, W. MacDonald, G. F. Neumark, M. C. Tamargo, and I. L. Kuskovsky, *Phys. Rev. B* **77**, 155314 (2008).
- ⁵Y. Gu, I. L. Kuskovsky, M. van der Voort, G. F. Neumark, X. Zhou, and M. C. Tamargo, *Phys. Rev. B* **71**, 045340 (2005).
- ⁶M. C. Kuo, C. S. Yang, P. Y. Tseng, J. Lee, J. L. Shen, W. C. Chou, Y. T. Shih, C. T. Ku, M. C. Lee, and W. K. Chen, *J. Cryst. Growth* **242**, 533 (2002).
- ⁷K. Suzuki, U. Neukirch, J. Gutowski, N. Takojima, T. Sawada, and K. Imai, *J. Cryst. Growth* **184–185**, 882 (1998).
- ⁸I. L. Kuskovsky, Y. Gu, Y. Gong, H. F. Yan, J. Lau, I. C. Noyan, G. F. Neumark, O. Maksimov, X. Zhou, M. C. Tamargo, V. Volkov, Y. Zhu, and L. Wang, *Phys. Rev. B* **73**, 195306 (2006).
- ⁹W. Lin, S. P. Guo, M. C. Tamargo, I. L. Kuskovsky, C. Tian, and G. F. Neumark, *Appl. Phys. Lett.* **76**, 2205 (2000).
- ¹⁰D. J. Chadi, *Phys. Rev. Lett.* **72**, 534 (1994).
- ¹¹D. Segev and S.-H. Wei, *Phys. Rev. B* **68**, 165336 (2003).
- ¹²S.-H. Wei and A. Zunger, *Appl. Phys. Lett.* **72**, 2011 (1998).
- ¹³Q. Zhang, A. Shen, I. L. Kuskovsky, and M. C. Tamargo, *J. Appl. Phys.* **110**, 034302 (2011).
- ¹⁴A. Luque and A. Marti, *Phys. Rev. Lett.* **78**, 5014 (1997).
- ¹⁵I. L. Kuskovsky, C. Tian, G. F. Neumark, J. E. Spanier, I. P. Herman, W. C. Lin, S. P. Guo, and M. C. Tamargo, *Phys. Rev. B* **63**, 155205 (2001).
- ¹⁶I. L. Kuskovsky, W. MacDonald, A. O. Govorov, L. Mouroukh, X. Wei, M. C. Tamargo, M. Tadic, and F. M. Peeters, *Phys. Rev. B* **76**, 035342 (2007).
- ¹⁷U. Manna, I. C. Noyan, Q. Zhang, I. F. Salakhutdinov, K. A. Dunn, S. W. Novak, R. Moug, M. C. Tamargo, G. F. Neumark, and I. L. Kuskovsky, *J. Appl. Phys.* **111**, 033516 (2012).
- ¹⁸A. A. Darhuber, P. Schittenhelm, V. Holy, J. Stangl, G. Bauer, and G. Abstreiter, *Phys. Rev. B* **55**, 15652 (1997).
- ¹⁹N. Faleev, K. Pavlov, M. Tabuchi, and Y. Takeda, *Jpn. J. Appl. Phys.* **38**, 818 (1999).
- ²⁰V. Holy, A. A. Darhuber, G. Bauer, P. D. Wang, Y. P. Song, C. M. S. Torres, and M. C. Holland, *Phys. Rev. B* **52**, 8348 (1995).
- ²¹V. Holý, G. Springholz, M. Pinczolits, and G. Bauer, *Phys. Rev. Lett.* **83**, 356 (1999).
- ²²V. Holý, J. Stangl, G. Springholz, M. Pinczolits, G. Bauer, I. Kegel, and T. H. Metzger, *Physica B* **283**, 65 (2000).
- ²³I. R. Sellers, V. R. Whiteside, I. L. Kuskovsky, A. O. Govorov, and B. D. McCombe, *Physica E* **40**, 1819 (2008).
- ²⁴G. S. Solomon, J. A. Trezza, A. F. Marshall, and J. J. S. Harris, *Phys. Rev. Lett.* **76**, 952 (1996).
- ²⁵Y. Gong, F. Y. Hanfei, I. L. Kuskovsky, Y. Gu, I. C. Noyan, G. F. Neumark, and M. C. Tamargo, *J. Appl. Phys.* **99**, 064913 (2006).
- ²⁶F. Hatami, M. Grundmann, N. N. Ledentsov, F. Heinrichsdorff, R. Heitz, J. Böhrer, D. Bimberg, S. S. Ruvimov, P. Werner, V. M. Ustinov, P. S. Kop'ev, and Z. I. Alferov, *Phys. Rev. B* **57**, 4635 (1998).
- ²⁷N. N. Ledentsov, J. Böhrer, M. Beer, F. Heinrichsdorff, M. Grundmann, D. Bimberg, S. V. Ivanov, B. Y. Meltser, S. V. Shaposhnikov, I. N. Yasievich, N. N. Faleev, P. S. Kopev, and Z. I. Alferov, *Phys. Rev. B* **52**, 14058 (1995).
- ²⁸B. Roy, A. Shen, M. Tamargo, and I. Kuskovsky, *J. Electron. Mater.* **40**, 1775 (2011).
- ²⁹V. A. Shuvayev, I. L. Kuskovsky, L. I. Deych, Y. Gu, Y. Gong, G. F. Neumark, M. C. Tamargo, and A. A. Lisyansky, *Phys. Rev. B* **79**, 115307 (2009).

- ³⁰M. C. K. Cheung, A. N. Cartwright, I. R. Sellers, B. D. McCombe, and I. L. Kuskovsky, *Appl. Phys. Lett.* **92**, 032106 (2008).
- ³¹Y. Gu, I. L. Kuskovsky, and G. F. Neumark, in *Wide Bandgap Light Emitting Materials and Devices*, edited by G. F. Neumark, I. L. Kuskovsky, and H. Jiang (Wiley-VCH, 2007), p. 147.
- ³²R. Passler, *J. Appl. Phys.* **83**, 3356 (1998).
- ³³R. Passler, E. Griebel, H. Riepl, G. Lautner, S. Bauer, H. Preis, W. Gebhardt, B. Buda, D. J. As, D. Schikora, K. Lischka, K. Papagelis, and S. Ves, *J. Appl. Phys.* **86**, 4403 (1999).
- ³⁴S. Sanguinetti, M. Henini, M. Grassi Alessi, M. Capizzi, P. Frigeri, and S. Franchi, *Phys. Rev. B* **60**, 8276 (1999).
- ³⁵Z. Y. Xu, Z. D. Lu, X. P. Yang, Z. L. Yuan, B. Z. Zheng, J. Z. Xu, W. K. Ge, Y. Wang, J. Wang, and L. L. Chang, *Phys. Rev. B* **54**, 11528 (1996).
- ³⁶D. Gammon, S. Rudin, T. L. Reinecke, D. S. Katzer, and C. S. Kyono, *Phys. Rev. B* **51**, 16785 (1995).
- ³⁷J. Lee, E. S. Koteles, and M. O. Vassell, *Phys. Rev. B* **33**, 5512 (1986).
- ³⁸N. Takojima, Y. Ishizuka, I. Tsubono, N. Kimura, K. Suzuki, T. Sawada, and K. Imai, *J. Cryst. Growth* **159**, 489 (1996).
- ³⁹P. W. Yu, *Solid State Commun.* **43**, 953 (1982).
- ⁴⁰P. J. Dean, D. C. Herbert, C. J. Werkhoven, B. J. Fitzpatrick, and R. N. Bhargava, *Phys. Rev. B* **23**, 4888 (1981).
- ⁴¹G. Bacher, C. Hartmann, H. Schweizer, T. Held, G. Mahler, and H. Nickel, *Phys. Rev. B* **47**, 9545 (1993).
- ⁴²S. Weber, W. Limmer, K. Thonke, R. Sauer, K. Panzlaff, G. Bacher, H. P. Meier, and P. Roentgen, *Phys. Rev. B* **52**, 14739 (1995).
- ⁴³Y.-H. Wu, K. Arai, and T. Yao, *Phys. Rev. B* **53**, R10485 (1996).
- ⁴⁴H. D. Sun, S. Calvez, M. D. Dawson, J. A. Gupta, G. C. Aers, and G. I. Sproule, *Appl. Phys. Lett.* **89**, 101909 (2006).
- ⁴⁵P. W. Yu and M. Cardona, *Fundamental of Semiconductor* (Springer-Verlag, Berlin, 1999).
- ⁴⁶Y. Gu, I. L. Kuskovsky, M. van der Voort, G. F. Neumark, X. Zhou, M. Munoz, and M. C. Tamargo, *Phys. Status Solidi B* **241**, 515 (2004).
- ⁴⁷U. E. H. Laheld, F. B. Pedersen, and P. C. Hemmer, *Phys. Rev. B* **52**, 2697 (1995).
- ⁴⁸P. Michler, A. Hangleiter, M. Moser, M. Geiger, and F. Scholz, *Phys. Rev. B* **46**, 7280 (1992).
- ⁴⁹J. D. Cuthbert and D. G. Thomas, *Phys. Rev.* **154**, 763 (1967).
- ⁵⁰K. Watanabe, M. T. Litz, M. Korn, W. Ossau, A. Waag, G. Landwehr, and U. Schussler, *J. Appl. Phys.* **81**, 451 (1997).
- ⁵¹M. T. Litz, K. Watanabe, M. Korn, H. Röss, U. Lünz, W. Ossau, A. Waag, G. Landwehr, T. Walter, B. Neubauer, D. Gerthsen, and U. Schüssler, *J. Cryst. Growth* **159**, 54 (1996).